Deep-Sea Research II ▮ (▮▮▮▮) ▮▮▮–▮▮▮

Contents lists available at ScienceDirect

Deep-Sea Research II

journal homepage: www.elsevier.com/locate/dsr2

Modeling tides in Monterey Bay, California

Xiaochun Wang [a,b], Yi Chao [a,*], Changming Dong [c], John Farrara [a,b], Zhijin Li [a], James C. McWilliams [c], Jeffrey D. Paduan [d], Leslie K. Rosenfeld [d]

[a] M/S 300-323, Jet Propulsion Laboratory, California Institute of Technology, 4800 Oak Grove Dr., Pasadena, CA 91109, USA
[b] Raytheon ITSS, 299 North Euclid Ave., Suite 500, Pasadena, CA 91101, USA
[c] IGPP, UCLA, 405 Hilgard Ave., Los Angeles, CA 90095, USA
[d] Department of Oceanography, Naval Postgraduate School, Monterey, CA 93943, USA

ARTICLE INFO

Article history:
Accepted 17 August 2008

Keywords:
Monterey Bay
Barotropic tides
Baroclinic tides
Modeling
Energy flux
High-frequency radar

ABSTRACT

In the process of developing a tide-permitting coastal ocean forecasting system, tidal signals are added to an oceanic general circulation model for Monterey Bay, California. The model, which is configured from the regional ocean modeling system (ROMS), has three one-way nested domains with the finest resolution of 1.6 km in the horizontal direction and 32 levels in the vertical direction. In present research, the tidal simulation of the system is validated against tide gauges, ADCP current observations, high-frequency radar surface-current observations, and compared with the output from two barotropic tidal models. The results indicate that the barotropic tides from the model compare well with observations in terms of sea-surface height, with discrepancies in amplitude of less than 10% of the amplitude of the most energetic M_2 constituent. However, the discrepancy for the barotropic tidal currents can reach 30% among models with similar accuracy in sea-surface height. The generation and propagation of baroclinic tides associated with the Monterey Submarine Canyon are qualitatively reproduced by the model with weaker strength. The surface tidal current simulation is improved, especially in terms of magnitude, when the model has a more realistic stratification through changes in both barotropic and baroclinic tidal currents.

1. Introduction

There have been numerous efforts using general circulation models to simulate tides around Monterey Bay, California. Rosenfeld et al. (1999) extended the work of Petruncio (1996) to include realistic bathymetry in three-dimensional tidal simulations of the region. Petruncio et al. (2002) numerically experimented with various submarine canyon scenarios, including a Monterey Submarine Canyon-like configuration, and demonstrated that the generation and propagation of baroclinic tides are very sensitive to the slope of the canyon floor. Rosenfeld et al. (2008) validated their Monterey Bay tidal simulation by comparing their output with tide gauges, bottom pressure gauges, and current measurements. Numerical experiments with constant density and uniform stratification were conducted to explore the relationship between stratification and tides. With the availability of present-day computing power, a high-resolution (270 m within Monterey Bay) and non-hydrostatic model was used in Jachec et al. (2006) to simulate tides in the region. The output from their model compares well with the observations in terms of the level of baroclinic tidal activity. This indicates that small-scale topographic features need to be represented in order to achieve a realistic strength of baroclinic tidal activity. In all these simulations, either a constant density or a horizontally uniform stratification was used. The models were also not forced by atmospheric forcing fields (wind stress, heat flux, evaporation minus precipitation).

From the perspective of coastal ocean forecasting, the presence of tides poses a challenge because the interaction of barotropic tides and bathymetry and the interaction of tides with variability in other frequency bands can cause complex flow patterns (e.g., Rainville and Pinkel, 2006). During August 2003, the field experiment adaptive ocean sampling network-II (AOSN-II) was conducted in Monterey Bay. The field experiment brought together a number of disparate observing platforms, such as autonomous underwater vehicles, gliders, moorings, aircrafts, and ships. There were also two real-time oceanic data assimilation and forecasting systems that provided forecasts for the region. Neither of the systems included tides at that time; thus, the forecasting was non-tidal. However, the Monterey Submarine Canyon can generate and trap baroclinic tides (Gordon and Marshall, 1976; Petruncio et al., 1998; Kunze et al., 2002). The breaking of

* Corresponding author. Tel.: +1 818 354 8168; fax: +1 818 393 6720.
E-mail address: ychao@jpl.nasa.gov (Y. Chao).

0967-0645/$ - see front matter © 2008 Elsevier Ltd. All rights reserved.
doi:10.1016/j.dsr2.2008.08.012

baroclinic tides and/or waves can cause strong turbulence dissipation in the canyon head (Carter and Gregg, 2002) and shelf region (Carter et al., 2005). There are also internal hydraulic jumps (Lien and Gregg, 2001) and solitary waves (Carter et al., 2005) that are associated with tides and cause strong dissipation and elevated diapycnal mixing in the region. It should be mentioned that Gregg et al. (2005) made corrections regarding some figures and numbers presented in Kunze et al. (2002) and Carter and Gregg (2002) because of an instrument problem. Surface-current observations using high-frequency radar (HF radar) also indicate that currents associated with semidiurnal baroclinic tides can reach 15 cm s^{-1}, comparable with wind-forced currents (Paduan and Cook, 1997). After the AOSN-II experiment, tidal signals were added to the three-domain nested regional ocean modeling system (ROMS) for Monterey Bay, which was one of the forecasting models used. In this research, the tidal simulation is validated against the tide gauges and current observations. The features of barotropic and baroclinic tides in the region are discussed. The sensitivity of the tide simulation to stratification is investigated through numerical experiments. Besides constant density and uniform stratification, time-dependent stratification and flow fields are included in these numerical experiments.

For a small region such as Monterey Bay, the tidal signal can be added to a primitive equation model through boundary conditions; Earth tide and astronomical tide potential can be ignored following the practice of Foreman et al. (1993). This was the approach used in this work. Besides the tidal forcing along the boundaries, the model is also forced by atmospheric forcing fields at the surface. Thus, both spatially variable stratification and subtidal variability are represented in the model. For the simulation of barotropic tides alone, especially if the goal is to simulate sea-surface height, atmospheric forcing can be neglected. This point is well established by numerous studies simulating tides in other parts of the world's oceans (e.g., Flather, 1976; Cummins and Oey, 1997; He and Wilkin, 2006) and Monterey Bay in particular (Rosenfeld et al., 2008). The interaction of barotropic tides and topography can make the flow pattern very complex in the presence of time-dependent stratification and mesoscale currents. However, for many applications of an operational coastal ocean forecasting system, it is desirable to simulate tides directly instead of providing a non-tidal solution. Another motivation for developing a tide-permitting circulation model is that the temperature, salinity, and current data collected by moving platforms (e.g., gliders or autonomous underwater vehicles) contain both the tidal signal and non-tidal variability. To remove the tidal signal (detide) from the data of a moving platform is a nontrivial process. Assimilating these data into a non-tidal model could introduce additional errors. Thus, the present research serves as a necessary first step toward the development of a tide-permitting forecasting system. More detailed analysis of the interaction of tides and mesoscale fields is beyond the scope of present research and left for future studies.

2. Model configuration and tidal analysis method

2.1. Model configuration

A three-domain, one-way nested model was configured for Monterey Bay, California, to do real-time data assimilation and forecasting for the AOSN-II experiment during August 2003 (Li et al., 2008a, b). The oceanic general circulation model used is the ROMS, which is a community model designed for coastal applications (Shchepetkin and McWilliams, 2005). The model uses a generalized vertical coordinate following the bottom topography (Song and Haidvogel, 1994). Compared with the traditional sigma-coordinate system, this vertical coordinate system provides more flexibility in choosing vertical levels in specific vertical domains, such as the bottom boundary layer or surface mixed layer. A curvilinear coordinate following the coastal line is used in the horizontal direction. The bottom topography of the nested model is from Smith and Sandwell (1997). The bathymetry from Smith and Sandwell (1997) is smoothed using a Hanning filter to make sure the r-factor ($\delta H/2H$, H is bathymetry) is less than 0.2, which is an empirical criterion to compute pressure gradient force accurately (Beckmann and Haidvogel, 1993). The smooth can be done reiteratively and for selected regions.

The model explicitly represents the time evolution of the free surface and has open lateral boundary conditions to allow the exchange of information through boundaries (Marchesiello et al., 2001). The vertical mixing scheme is the K-profile parameterization scheme, which can accommodate some potentially important physics of ocean mixing (Large et al., 1994). The vertical diffusivity can change from 10^{-5} m^2 s^{-1} in the ocean interior to 10^{-2} m^2 s^{-1} in the surface boundary layer. The horizontal mixing scheme is the Laplacian scheme on z-level with a constant viscosity of 50 m^2 s^{-1} and diffusivity of 25 m^2 s^{-1}. Part of the horizontal mixing of the present configuration is also from the up-stream advection scheme (Shchepetkin and McWilliams, 2005).

Fig. 1 shows the three nested model domains. The outermost model domain (L0), which has the coarsest resolution, covers the US western coastal region from Southern California to Oregon. The intermediate model domain (L1) covers the Central and Northern California coast. The finest-resolution model domain (L2) zooms in on the Monterey Bay region. The nesting of the model domains is realized through the Adaptive Grid Refinement in Fortran (AGRIF) package, which is based on the use of pointers (Blayo and Debreu, 1999). Currently the nesting between L0 and L1 (and between L1 and L2) is one way. The coarse-resolution domain provides boundary conditions for the fine-resolution domain and the solution of the fine-resolution domain does not feed back to the coarse-resolution domain. This online nesting allows the three domains to run simultaneously and exchange boundary conditions at every time step. This is in contrast to the offline nesting that stops and restarts the nested domains at a fixed time internal. The AGRIF ROMS has been systematically tested by Penven et al. (2006). The testing shows that the package can provide a continuous transition from the coarse resolution to fine resolution solution. Table 1 lists the domains and details of our nested model. The horizontal resolutions for the L0, L1, and L2 domains are 15.7, 5.0, and 1.6 km, respectively. All three model domains have 32 vertical levels following the bottom topography. The Flather (1976) boundary condition is used along the open boundaries (western, southern, and northern boundaries) for the normal barotropic velocity of the L0 domain to allow the propagation of tide signals into the model domain. The Chapman (1985) boundary condition is used for sea-surface height along the open boundaries. For the Chapman boundary condition, it is assumed that the dominant wave packet approaching the boundary is non-dispersive gravity waves and the phase speed is estimated based on depth. The detailed boundary conditions for the barotropic velocity and sea-surface height are shown in Table 2. For baroclinic velocity, temperature, and salinity, the adaptive open-boundary conditions are used along the western, southern, and northern boundaries (Marchesiello et al., 2001). The adaptive open-boundary conditions treat inward and outward wave packets differently. When the phase speed estimated from the interior solution is outward, these wave packets can propagate out of the model domain (Orlanski, 1976; Raymond and Kuo, 1984). When the phase speed is inward, the interior solution at the boundary is relaxed to the exterior solution (either from a

Please cite this article as: Wang, X., et al., Modeling tides in Monterey Bay, California. Deep-Sea Research II (2008), doi:10.1016/j.dsr2.2008.08.012

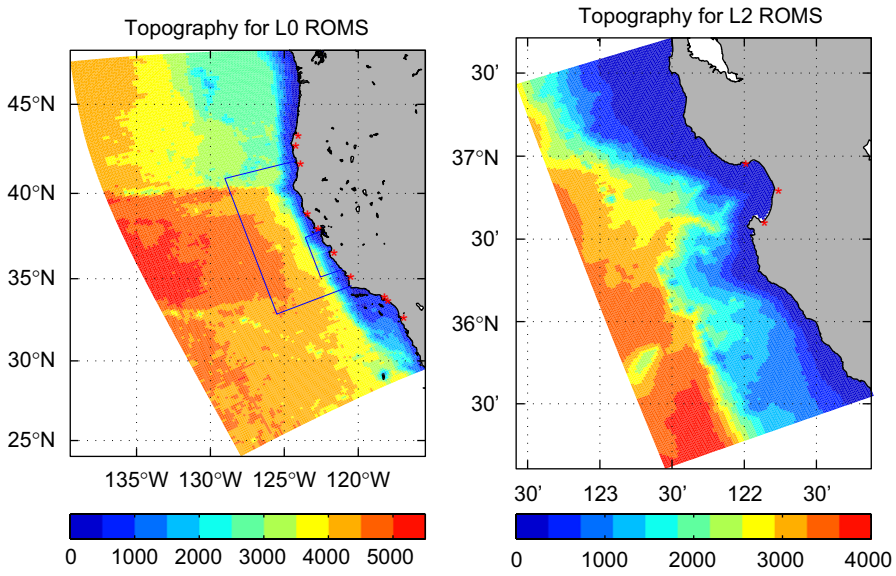

Fig. 1. Topography in the coarsest-resolution model domain (L0, left), and the topography in the finest-resolution model domain (L2, right) of the three-domain nested model. The boundaries of the nested domains are also shown as black boxes in the left panel. The red stars show the tide gauges used to validate the model tidal solution. There are 10 gauges for the L0 domain and three gauges for the L2 domain.

Table 1
The maximum and minimum depths, horizontal range in latitude and longitude, resolutions, and time steps of the three-domain nested ROMS model for the US western coast

	Max. depth	Min. depth (m)	Latitude (N)	Longitude (W)	Resolution (km)	Time step (s)
L0 model	5346.5	285.0	24.0–47.9	139.5–115.6	15.7	900
L1 model	4780.8	100.0	32.9–41.7	129.0–120.0	5.0	300
L2 model	3943.9	10.2	35.1–37.8	123.6–121.1	1.6	100

Table 2
Boundary conditions used for sea-surface height and barotropic velocity for the three-domain one-way nested ROMS model of the US western coast

	Open boundary	Closed boundary
Sea-surface height	Chapman	Zero gradient
Tangential velocity	Oblique radiation	Free slip
Normal velocity	Flather condition	Zero

large domain model or from a climatological field) with a specified time scale of three days. This implies that the baroclinic tidal signal within L2 model domain are mostly generated locally and not influenced much by the baroclinic tidal signal generated in the L0 and L1 model domains. Using 16 processors on an SGI Altix 3000 computer, it takes 1 min of wall-clock time to integrate the nested model for one hour.

The topographic features in the L0 model domain (left panel of Fig. 1) include a very narrow continental margin on the order of 50–100 km wide. Along 40°N, there is a topographic feature called the Mendocino Escarpment. In a band from 135 to 125°W, the ocean depth shallows abruptly by around 1000 m from south to north. This feature is known to be associated with strong baroclinic tide activity (Althaus et al., 2003). The most prominent topographic feature in the L2 model domain is the Monterey Submarine Canyon cutting into Monterey Bay. This unique feature enhances the baroclinic tide activity in the region (e.g., Petruncio et al., 1998; Kunze et al., 2002) and also makes Monterey Bay one of the most studied regions of the US West Coast. It should be noted that even with our finest horizontal resolution of 1.6 km in the L2 model domain, some complexities in the bathymetry of the Monterey Submarine Canyon cannot be fully represented.

The non-tidal model configuration was tested during the AOSN-II experiment. The modifications we made here were to add tidal boundary conditions in the barotropic transport and sea-surface height along the western, southern, and northern boundaries. The Earth tide, load tide, and astronomical tide-generating potential have been neglected since the influence of these factors are minor in regional tidal simulations (Foreman et al., 1993). The presence of time-dependent stratification and subtidal variability poses some challenges for tidal simulation. For the present model configuration, the time step needs to be reduced by a factor of three to accommodate the enhanced semidiurnal and diurnal variability associated with tides. Based on CFL condition, the original and the reduced time step can accommodate a maximum velocity or phase speed of 5.3 and 16 m s^{-1}, respectively. The 5.3 m s^{-1} seems plausible since it is much larger than the typical current speed. However, without reducing time step, the model will blow up in a few steps, indicating the blowup is related with the barotropic part. The CFL condition is only a necessary condition for numerical stability with explicit scheme. Quite often a time step satisfying CFL condition can not guarantee numerical stability.

2.2. Model forcing

The tidal forcing is obtained from a global inverse barotropic tidal model (TPXO.6) (Egbert and Erofeeva, 2002; Egbert et al.,

Please cite this article as: Wang, X., et al., Modeling tides in Monterey Bay, California. Deep-Sea Research II (2008), doi:10.1016/j.dsr2.2008.08.012

1994), which has a horizontal resolution of 0.25° and uses an inverse modeling technique to assimilate satellite altimetry cross-over observations. Eight major tide constituents of diurnal and semidiurnal frequencies (M_2, K_1, O_1, S_2, N_2, P_1, K_2, Q_1, ordered by their amplitudes in the region) are used for our boundary condition. The TPXO.6 solution is available from http://www.coas.oregonstate.edu/research/po/research/tide/. The barotropic transport from the TPXO.6 solution is adjusted using ROMS bathymetry because the bathymetry fields from ROMS and TPXO.6 are different. To account for the 18.6-year cycle of astronomical tide-generating potential, nodal correction (Foreman, 1977) is applied to the sea-surface height and barotropic transports of the TPXO.6 solution. The nodal correction is done for July 26, 2003, 3GMT. These two procedures proved to be important in achieving an accurate barotropic tidal solution. The simulation period is August 2003, which is the duration of the AOSN-II field experiment. During this field experiment, the non-tidal version of the model was used to conduct experimental coastal ocean operational forecasting. The atmospheric forcing consists of the wind stress, heat flux, and freshwater flux from the Coupled Ocean/Atmosphere Mesoscale Prediction System (COAMPS^{TM}, Hodur, 1997). For the US West Coast, COAMPS^{TM} has a quadruple nested-grid configuration with horizontal resolutions of 81, 27, 9, and 3 km from the coarsest to the finest grid. The outputs from 27, 9, and 3 km model domains are used to force the L0, L1, and L2 ROMS model, respectively (Li et al., 2008b). The latent and sensible heat fluxes are computed using the surface air temperature, relative humidity, 10 m wind from COAMPS^{TM}, and sea-surface temperature from ROMS based on the bulk formula (Kondo, 1975). The wind stress is computed from the 10 m wind using the formula of Large and Pond (1982).

2.3. Tidal analysis

For our numerical experiments, the model is integrated for one month and the tidal parameters (phase and amplitude) are then estimated to compare with observations. The T_TIDE package (Pawlowicz et al., 2002) is used for the tidal harmonic analysis. The package is the MATLAB version of the tidal harmonic analysis software in Fortran (Foreman, 1977, 1978). The software does a least-square fit to tidal constituents with certain frequencies. When the time series is too short, not all the major constituents can be resolved and there are large uncertainties associated with the estimation. The subtle aspects in estimating tidal parameters are discussed in Rosenfeld et al. (2008). When the data are one month long with hourly sampling, the semidiurnal constituent pair K_2 and S_2 and the diurnal constituent pair K_1 and P_1 cannot be resolved explicitly in the frequency domain and be picked up automatically by the T_TIDE package if the default Rayleigh criterion with value 1 is used. Instead of using the inference method, which specifies the ratios of amplitudes between K_1 and P_1 and between K_2 and S_2, we only estimate the eight constituents using T_TIDE by specifying them directly. The method is justified since the model is only forced by these constituents. The current is also 8–28-hour band-pass filtered using Lanczos-window cosine filter (Emery and Thomson, 2004) before the tidal harmonic analysis is applied. Our analysis shows that for sea-surface height, the tidal amplitude and phase estimation with one month of model output and those with one year of model output are approximately the same. For tidal currents, specifying tidal constituents and conducting 8–28-hour band-pass filtering also can reduce the error in estimation.

Following the convention of tidal harmonic analysis used in T_TIDE, the tidal motion of sea-surface height (and other scalar variables such as pressure and density) is represented as an amplitude and phase. The phase is relative to the Greenwich meridian, in units of degrees. The tidal current is represented as an ellipse that has four parameters: the length of the semi-major axis, the length of the semi-minor axis, the inclination angle from due east, and the phase. When plotting the tidal current ellipses of a constituent, the phase is shown as the direction of the current when the sea-surface height at the Monterey tide gauge reaches its maximum for the constituent (Rosenfeld et al., 2008). The barotropic current is the depth-averaged current of all vertical levels of the model. The baroclinic current is the total current minus the barotropic current at each time step. The methods used to compute depth-integrated baroclinic tidal energy and energy flux are presented in Appendix A.

3. Validation of barotropic tides

3.1. Validation of sea-surface height

Forced by tidal signals along the open boundaries, the nested model can reproduce the barotropic tides along the US West Coast very well. In the L0 model domain, 10 tide gauges are used to validate the solution. These 10 tide gauges are distributed from Southern California to Oregon (red stars in the left panel of Fig. 1). The data for these tide gauges are obtained from the website (http://tidesonline.nos.noaa.gov) of the National Ocean Services. The tidal amplitude and phase are estimated using hourly sea-surface height data for 2003. For tide gauges without hourly data for 2003, the amplitude and phase from the archive of the National Ocean Services are used. Fig. 2 compares the amplitude and phase of eight tide constituents. The RMS discrepancy between observed and model simulated amplitude varies from 4.6 cm for M_2 to 0.2 cm for Q_1. Overall, the total discrepancy of amplitude can be measured by the root of summed squares (RSS, Shum et al., 1997) of tide amplitudes, which is 5.41 cm for these 10 stations. The RMS discrepancy of tidal phase is generally less than 7°, which translates to 14 min for the semidiurnal tides and 28 min for the diurnal tides. In the L2 model domain (Fig. 3), the RSS of tide amplitudes is 3.61 cm, which is more accurate than that of the L0 model domain. The higher accuracy of the tidal solution in the L2 model domain is associated with the better representation of coastal geometry and bottom topography on the refined grid. The phase discrepancy between model and tide gauges is generally less than 6° except for Q_1, which has a small amplitude (a few centimeters) in the region and for which large errors may be expected in the tidal parameter estimations. The tidal solution of sea-surface height from Rosenfeld et al. (2008) has a standard error of 2.23 cm, which is more accurate than our solution. This is because the model used by Rosenfeld et al. (2008) has a domain size of 1.5°Lat. × 1.5°Long. and a regional 1/12° resolution TPXO solution is used as the boundary condition. Our L0 model domain has a domain size of 24°Lat. × 24°Long. on which a global 0.25° resolution TPXO solution is used. If the 1/12° resolution TPXO solution is directly added to the L2 model domain, the RSS for sea-surface height for the L2 stand-alone run is reduced to 1.06 cm. The phase discrepancies between ROMS and the tide gauges are reduced to less than 1.5° in this case. Though the above ROMS model configured for the L2 domain alone can provide a more accurate barotropic tidal solution, the three-domain nested model can obtain adequate background information for a relatively larger domain which is needed for a real-time forecasting system. Since part of the goal of the present research is to validate the tidal solution for the three-domain nested forecasting system, the tide solution from the L2 stand-alone run is not analyzed further here.

Please cite this article as: Wang, X., et al., Modeling tides in Monterey Bay, California. Deep-Sea Research II (2008), doi:10.1016/j.dsr2.2008.08.012

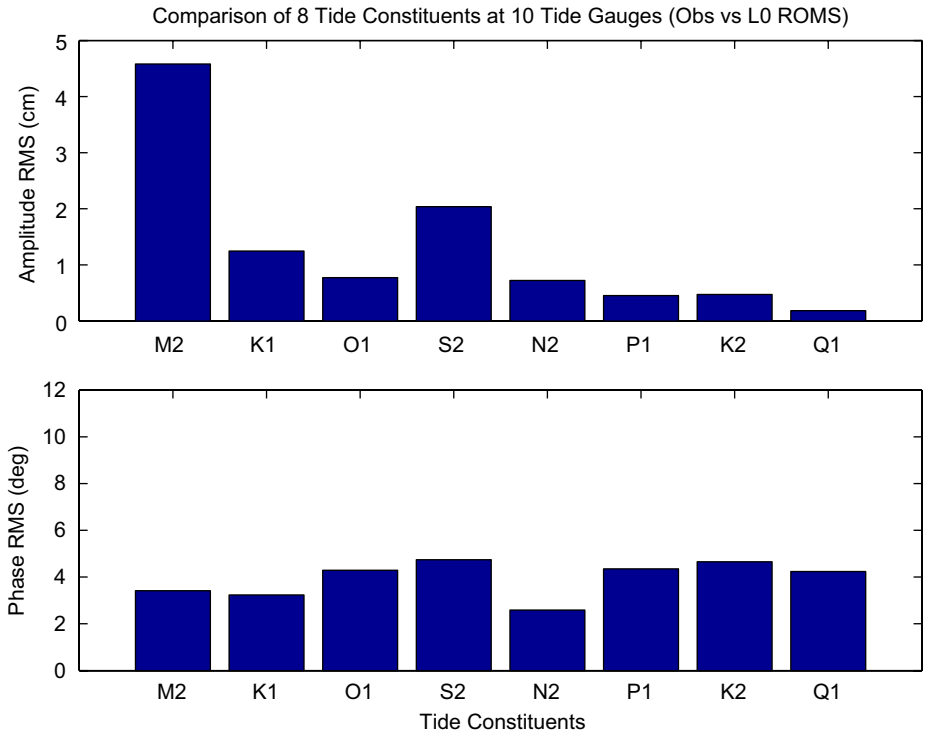

Fig. 2. The root-mean-square discrepancy of tidal amplitude and phase between 10 tide gauges and the L0 model output.

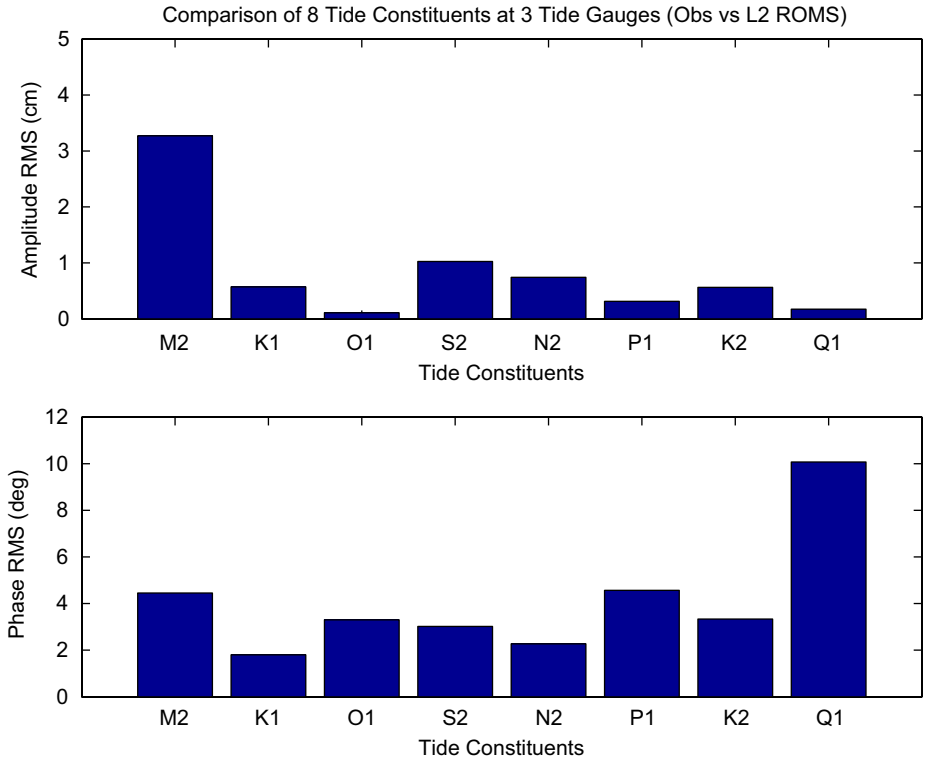

Fig. 3. The root-mean-square discrepancy of tidal amplitude and phase between three tide gauges and the L2 model output.

3.2. Comparison of tidal currents

Current observations that are long enough and cover the full depth of the water column, suitable for the purpose of tidal validation analysis, are very sparse. Here the barotropic tidal current from the L0 model domain is compared with the tidal current in the TPXO.6 solution because the TPXO.6 solution has a comparable horizontal resolution of 0.25° and assimilates altimetry observations (Table 3). In this comparison, the barotropic transport of the TPXO.6 solution is scaled by the ROMS bathymetry, not its original bathymetry. The RMS discrepancy for sea-surface height is shown for comparison. In the L0 model

Please cite this article as: Wang, X., et al., Modeling tides in Monterey Bay, California. Deep-Sea Research II (2008), doi:10.1016/j.dsr2.2008.08.012

Table 3
RMS discrepancy for the amplitude of sea-surface height, the length of the semi-major axis of tidal current ellipse of the TPXO.6 solution and the L0 ROMS output

	SSH (cm)		Semi-major axis (cm s^{-1})	
	M_2	K_1	M_2	K_1
RMS	2.79	1.23	0.65	0.37
Mean	47.56	33.33	2.98	0.71

The area mean of these variables from ROMS is also shown.

Table 4
RMS discrepancy for the amplitude of sea-surface height, the length of the semi-major axis of tidal current ellipse of the ADCIRC solution and the L2 ROMS output

	SSH (cm)		Semi-major axis (cm s^{-1})	
	M_2	K_1	M_2	K_1
RMS	6.67	2.64	1.01	1.82
Mean	51.29	38.17	3.66	0.98

The area mean of these variables from ROMS is also shown.

domain, the barotropic tidal current is generally along the coast. The magnitude of the M_2 tidal current, as measured by the area average of the length of semi-major axes of tidal current ellipses, is 3.0 cm s^{-1}. The percentage differences (as measured by RMS discrepancy divided by mean) for tidal current magnitude are 21% for M_2 and 52% for K_1, which are much larger than their counterparts for sea-surface height (6% for M_2 and 4% for K_1).

For the L2 model domain, the ROMS tidal current is compared with a relatively recent tidal database for the Eastern North Pacific produced by a finite element model with high resolution along the coast (Spargo et al., 2004). This model is a two-dimensional, depth-integrated form of the coastal hydrodynamic model (ADCIRC, advanced circulation, Luettich et al., 1992) and is also forced by the TPXO.6 solution along its open boundaries. In the Monterey Bay region (Table 4), both the ROMS model output and the ADCIRC solution indicate that the magnitude of the tidal current is enhanced with a mean magnitude of 3.7 cm s^{-1} for the M_2 constituent. Compared with the L0 model domain, the difference between the sea-surface height is large, with a percentage difference of 13% for the M_2 constituent. The percentage difference between the magnitude of tidal currents is generally over 30%. Thus the tidal solution from ROMS compares well with observations in terms of sea-surface height, while the comparison of its tidal currents with two barotropic tidal models indicates that large discrepancies (over 30%) can exist even though the difference in sea-surface height is small (less than 10%).

4. Barotropic and baroclinic tides in Monterey Bay

4.1. Barotropic tides

In this section, the features of the barotropic and baroclinic tides are analyzed for the L2 model domain. Though eight major tidal constituents are included in our tidal simulation, only the M_2 constituent is analyzed since the characteristic of tides in the region is mixed, predominantly semidiurnal (Petruncio et al., 1998). In the L2 model domain, the M_2 amplitude increases from 40 cm in the southwestern corner of the domain to 50 cm in the northeastern corner of the model domain (left panel of Fig. 4). The phase differences in the L2 domain are less than 15° and also indicate a northward propagation. The small-scale variability in the amplitude and phase, which is the surface manifestation of baroclinic tides (Ray and Mitchum, 1996), is associated with model stratification.

The barotropic tidal currents for M_2 are oriented along the shore in the open ocean and modified by bathymetric features in the coastal region (right panel of Fig. 4). The alongshore orientation of the tidal current is consistent with the mathematical analysis of Battisti and Clarke (1982). The magnitudes of the M_2 tidal currents are generally around 3−4 cm s^{-1}. Compared with other US coastal regions (such as the New England shelf; He and Wilkin, 2006), the California coast has a weak barotropic tidal current because the continental shelf is very narrow. The water depth drops to thousands of meters within tens of kilometers offshore. The tidal currents are enhanced to the north and south of the Monterey Submarine Canyon over the shallower bathymetry and undergo a change of direction of rotation from counter-clockwise to clockwise, which is a persistent feature of the barotropic tidal current even in the presence of different stratifications as shown in Section 5.

4.2. Baroclinic tidal energy and flux

The interaction of barotropic tides and topography can generate baroclinic tides (e.g., Baines, 1982). Details of the generated baroclinic tides also depend on stratification. Thus, these features should be discussed in the context of our model stratification, which is done in the next section. Fig. 5 shows the depth integrated baroclinic tidal energy and flux for the M_2 constituent. It should be noted that the Monterey Bay region is associated with enhanced baroclinic tidal energy, consistent with observations (Petruncio et al., 1998).

The energy flux distribution indicates that M_2 baroclinic tides can be generated locally both inside and outside Monterey Bay (Fig. 5). The baroclinic tides generated outside the bay can propagate into the bay along its southern and northern flanks. The unconventional curl structure of the energy flux around the bay (personal communication with Dr. E. Kunze), especially the northwestward energy flux around 36°30′N, 122°45′W and the northeastward to eastward flux around 36°48′N, 122°36′W, is probably associated with the baroclinic tide generation by sea mountains at 36°18′N, 122°36′W, and 36°45′N, 123°W, respectively. Baroclinic tides generated in the northern and southern flanks of the ridge along 36°15′N propagate away from the generation sites. In the enlarged figure for Monterey Bay (right panel of Fig. 5), baroclinic tides can propagate into the bay and reach the head of the Monterey Submarine Canyon. The features of baroclinic tidal energy flux are in qualitative agreement with observations (Kunze et al., 2002), though with somewhat smaller magnitude. The baroclinic tidal energy flux from the L2 model has a magnitude of about 500 W m^{-1} in the Monterey Bay region. The observed baroclinic tidal energy fluxes, however, have a magnitude ranging from 1000 to 2000 W m^{-1} with extreme magnitude around 5000 W m^{-1} (Kunze et al., 2002). It should be noted that the observed baroclinic tidal energy fluxes in Kunze et al. (2002) contain contributions from other semi-diurnal constituents besides M_2 and the observation was conducted during spring tide. The baroclinic tidal energy fluxes also vary by a factor of ten around the Monterey Submarine Canyon (Fig. 10 of Kunze et al., 2002). Though there are issues associated with sampling and changes in stratification in observational studies (Nash et al., 2005), the model may still underestimate the baroclinic tidal energy flux by a factor of two to ten. By using a model with a higher resolution of 270 m in the horizontal direction and 100 levels in the vertical direction, Jachec

Please cite this article as: Wang, X., et al., Modeling tides in Monterey Bay, California. Deep-Sea Research II (2008), doi:10.1016/j.dsr2.2008.08.012

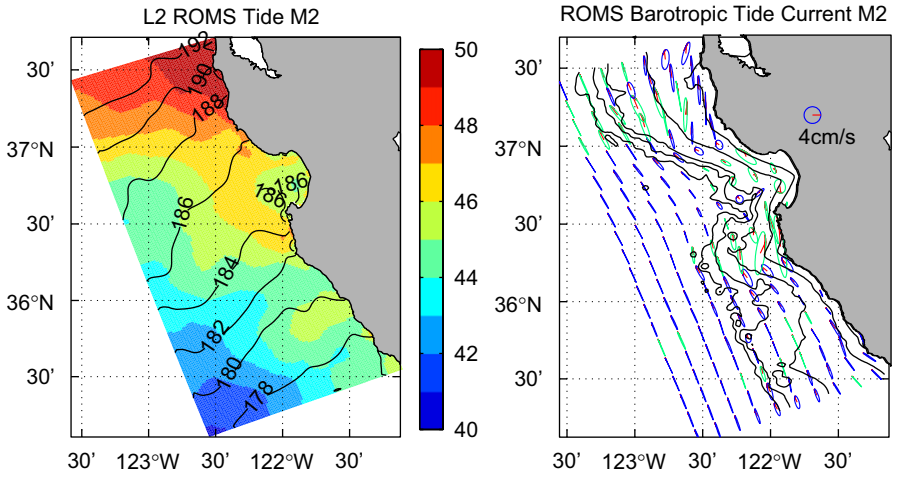

Fig. 4. The amplitude and phase of sea-surface height (left) and barotropic tidal current ellipses (right) for the M_2 constituent in the L2 model domain. A tidal current ellipse shows the length of the semi-major axis, the length of the semi-minor axis, and the inclination from due east. Blue ellipses mean that the tip of the current vector rotates counterclockwise, and green ellipses mean clockwise rotation. The red line in each ellipse shows the direction of the current when the sea-surface height at the Monterey station reaches its maximum. The magnitude of the tidal current is shown in the scale ellipse with the semi-major axis and the semi-minor axis having the same length as the label. The contours in the right panel show selected (50, 200, 1000, 1500, 2000 m) model isobaths.

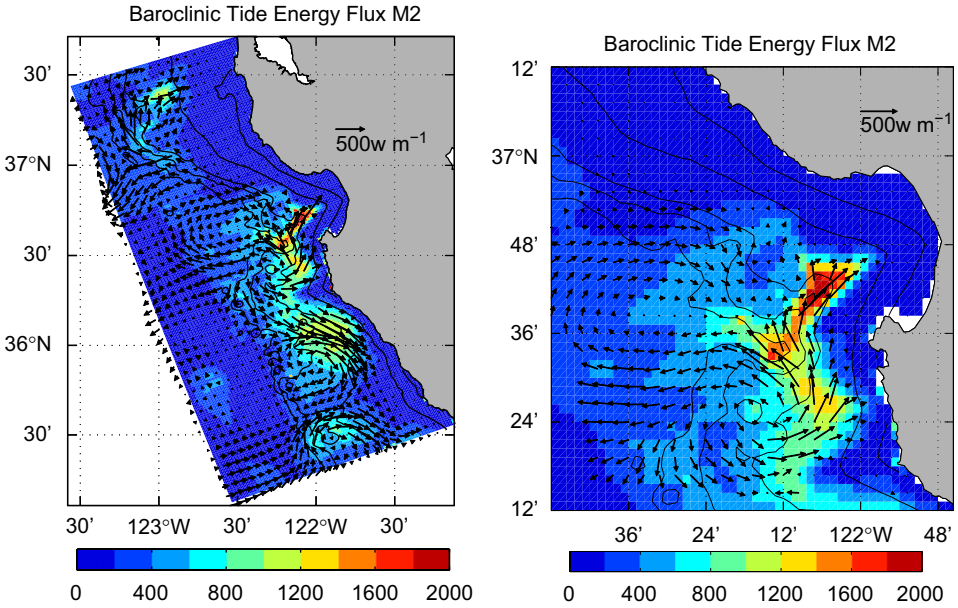

Fig. 5. The depth-integrated baroclinic tidal energy (in J m^{-2}) and energy flux (in W m^{-1}) for the M_2 constituent in the L2 model domain (left) and the enlarged Monterey Bay region (right). The color bar shows the depth-integrated baroclinic tidal energy. The contours show selected (50, 200, 1000, 1500, 2000 m) model isobaths.

et al. (2006) showed that the baroclinic tidal energy flux of their model is smaller than that of Kunze et al. (2002) by a factor of two. However, it is not plausible to use a model with that order of resolution to conduct real-time forecasting over a spatial domain comparable to ours. The sensitivity of the baroclinic tidal solution to resolution still needs to be explored further in order to find an optimal resolution for a model to use in real-time forecasting, which might depend on the bathymetric features to resolve (Holloway and Merrifield, 1999).

5. Sensitivity of tidal solution to stratification

The baroclinic tidal activity around Monterey Submarine Canyon appears to change in different seasons, implying the influence of stratification (Petruncio et al., 1998). Observations from HF radar reveal significant and robust baroclinic tidal signals in the surface currents (Paduan and Cook, 1997; Rosenfeld et al., 2008). Given the potential applications of surface-current forecasting, the sensitivity of surface tidal current to stratification is investigated here through numerical experiments.

5.1. Experiments with different stratifications

In order to analyze the sensitivity of surface tidal current simulation to stratification, a suite of four experiments is conducted and the simulated surface M_2 tidal currents are compared with the observations from HF radar. Fig. 6E shows the sea-surface tidal current ellipses for the M_2 constituent from HF-radar observations for August 2003. The major features include: (1) the magnitude of tidal current is greatly enhanced on the shelf region where the water depth is less than 200 m; (2) tidal currents at the head of the canyon and the southwestern

Please cite this article as: Wang, X., et al., Modeling tides in Monterey Bay, California. Deep-Sea Research II (2008), doi:10.1016/j.dsr2.2008.08.012

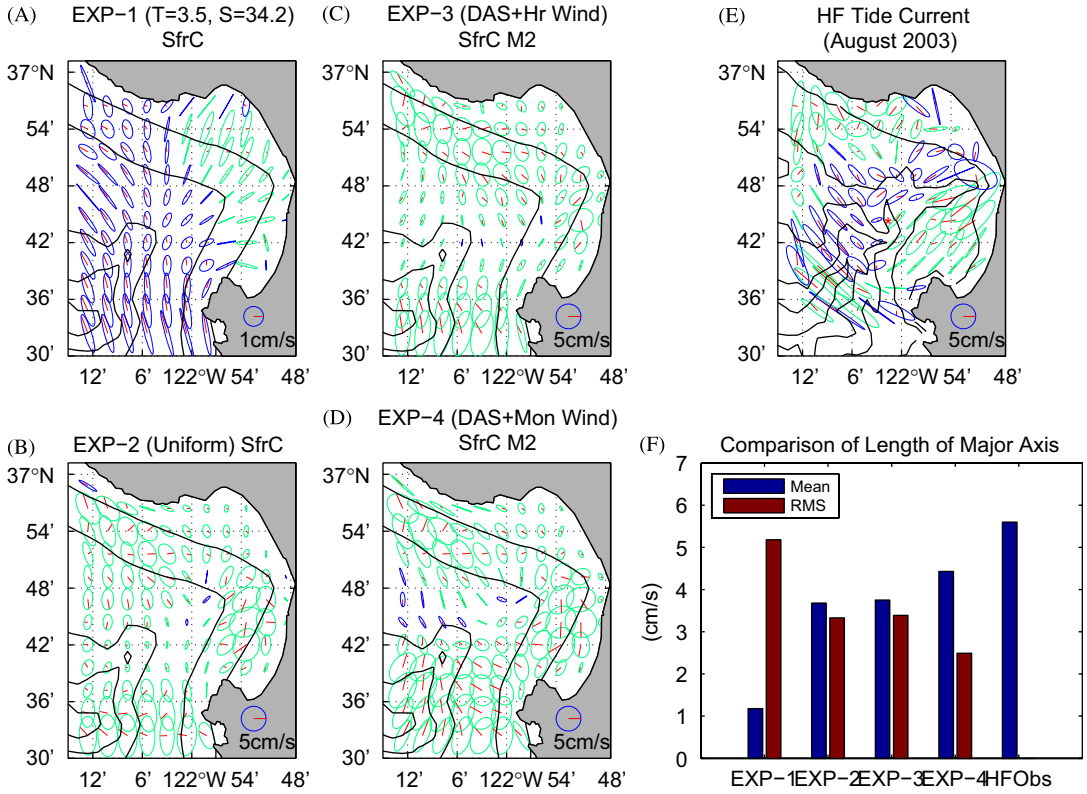

Fig. 6. Surface M_2 tidal current ellipses from four numerical experiments (A–D) and their comparison (F) with high-frequency radar observations of August 2003 (E). Experiment 1 starts from a constant temperature as 3.5 °C and a constant salinity as 34.2 psu and without atmospheric forcing. Experiment 2 starts from a horizontally uniform stratification profile and without atmospheric forcing. Experiment 3 starts from a data-assimilated initial condition of August 2003 and uses hourly wind-stress forcing. Experiment 4 starts from the same initial condition as Experiment 3 but uses monthly wind-stress forcing. Details are described in Section 5.1. The contours in (A–D) show selected (50, 200, 1000, 1500, 2000 m) model isobaths. (E) The surface tidal current ellipses from high-frequency coastal radar observations for August 2003. The red star in (E) shows the location of mooring 46092 (M1). The contours in (E) show selected (50, 200, 1000, 1500, 2000 m) isobaths interpolated to the model grid. (F) The root-mean-square discrepancy of the length of the semi-major axis between the model and high-frequency radar observations (red), and the area average of the length of the semi-major axis (blue). The area average of the length of the semi-major axis from observations is also shown in (F).

Table 5
Numerical experiments to analyze the sensitivity of surface tidal currents to stratification

	Exp. 1	Exp. 2	Exp. 3	Exp. 4
Initial condition	$T = 3.5$ °C, $S = 34.2$ psu	Uniform T, S	Data-assimilated	Data-assimilated
Atmo. forcing	N/A	N/A	Hourly forcing	Monthly forcing
Surface current (cm s^{-1})	1.18	3.68	3.28	4.24
Barotropic current (cm s^{-1})	1.18	2.49	2.69	2.90
Baroclinic current (cm s^{-1})	N/A	3.11	3.03	3.75
Baroclinic energy (J m^2)	N/A	270.09	332.13	357.77

The first row is the model initial condition. The second row is the temporal resolution of atmospheric forcing if there is any. The third row is the mean of the length of the semi-major axis of the surface tidal current ellipses for the M_2 constituent in the Monterey Bay region. The fourth row is the mean of the length of the semi-major axis of the barotropic tidal current ellipses. The fifth row is the mean of the length of the semi-major axis of the surface baroclinic tidal current ellipses. The sixth row is the mean baroclinic tidal energy.

entrance of the canyon (36°36′N, 122°6′W) are the largest; and (3) associated with the canyon, the rotation of the tidal current is counterclockwise. Table 5 shows the details of these four experiments and compares the area-averaged lengths of the semi-major axis of surface tidal current ellipses, barotropic tidal current ellipses, surface baroclinic tidal current ellipses, and depth-integrated baroclinic tidal energy in these four experiments. Area averages for the Monterey Bay region (36°30′N–37°N, 122°15′W–121°45′W) are presented. This region is shown in Fig. 6E and is chosen to coincide with the availability of HF-radar observations.

In Experiment 1, the model is integrated starting from an initial condition of constant temperature (3.5 °C) and salinity (34.2 psu) without atmospheric forcing. In Experiment 2, the model starts from an initial condition of uniform stratification in the model domain and without atmospheric forcing. The stratification profile is the Monterey Bay area average of the output of the four-times-daily data assimilation and forecasting system (Li et al., 2008b) for the period of August 2003. In Experiments 3 and 4, the same output of the data assimilation and forecasting system is averaged to obtain an estimate of oceanic conditions for August 2003. The model starts from this data-assimilated initial condition and is forced by tidal boundary condition and atmospheric forcing. The difference between Experiments 3 and 4 is that a monthly-mean wind-stress forcing is used in Experiment 4, while for Experiment 3 hourly wind-stress forcing is used. For the data-assimilated initial conditions of Experiments 3 and 4, the temperature and

Please cite this article as: Wang, X., et al., Modeling tides in Monterey Bay, California. Deep-Sea Research II (2008), doi:10.1016/j.dsr2.2008.08.012

salinity profiles are very close to observations with a monthly RMS difference in temperature of less than 0.5 °C, and the difference in salinity less than 0.1 psu (Chao et al., 2008) for independent mooring observation. All the analysis in the earlier sections uses the output from Experiment 4. It should be emphasized that all the four experiments were integrated for 800 hours. The hourly output from 49 to 800 hours is used in our tidal analysis, which also removes a linear trend. This procedure minimizes the influence from possible initial adjustment of the model.

From Experiments 1–4, the surface tidal current gradually improves with enhancements in the surface tidal current in the shelf region and the appearance of counterclockwise tidal current rotation associated with the submarine canyon (Fig. 6A–D). The improvement of the surface tidal current simulation is also obvious in the RMS discrepancy of the length of the simulated semi-major axes and HF-radar observations (Fig. 6F). The area-averaged length of the semi-major axis of surface tidal current ellipses is 5.8 cm s^{-1} from HF-radar observations. The area-averaged length of the simulated semi-major axis gradually increases from 1.18 cm s^{-1} for Experiment 1 to 4.24 cm s^{-1} for Experiment 4, because of the better representation of the stratification. The RMS discrepancy of the semi-major axes between the observation and model decreases from 5.18 cm s^{-1} for Experiment 1 to 2.76 cm s^{-1} for Experiment 4. In these four experiments, the fundamental difference is stratification, which is obtained through changes in initial conditions and atmospheric forcing fields. The magnitude of the surface M_2 tidal current from Experiment 4 is larger than that from Experiment 3 by 25%. Considering the fact that the hourly wind-stress forcing is used in Experiment 3, it may be concluded that the direct influence of wind-stress forcing to surface current at the semidiurnal frequency is small. It should be pointed out that the hourly wind-stress forcing does enhance the surface current at the diurnal frequency by several factors (figure ignored).

The complex correlation coefficient is also used to compare the model tidal current and HF-radar observation. As demonstrated in Kundu (1976), the complex correlation coefficient between two vector series $w_1(t)$ and $w_2(t)$

$$\rho = \frac{\langle w_1^*(t) w_2(t) \rangle}{\langle w_1^*(t) w_1(t) \rangle \langle w_2^*(t) w_2(t) \rangle} \quad (1)$$

can be used to analyze the relationship between them. In the above formula, the asterisk indicates the complex conjugate, and the angle bracket means the inner product with t being time. The magnitude of ρ gives the overall measure of correlation and its phase angle is the average counterclockwise angle of vector $w_2(t)$ with respect to vector $w_1(t)$. The phase angle is meaningful only if the magnitude of complex correlation coefficient is high. Fig. 7 shows the magnitude of complex correlation coefficient of model M_2 surface tidal current and HF-radar observation. The Monterey Bay area-averaged magnitude of complex correlation coefficient are 0.65, 0.74, 0.71, 0.72 for Experiments 1–4, respectively, which indicates the improvement of tidal current simulation with the presence of relatively realistic stratification. The magnitude of complex correlation coefficient has large values in the shelf region for Experiments 2–4. The region along the submarine canyon has small magnitude of complex correlation coefficient, which indicates that the baroclinic tide activity associated with the canyon is not simulated very well (Fig. 7B–D). Though the Experiment 1 underestimates the magnitude of surface tidal current by a factor of five, the counterclockwise rotation of surface tidal current is responsible for the large magnitude of complex correlation coefficient around the canyon (Fig. 7A). Our Monte Carlo simulation for complex correlation coefficient by randomly generating tidal current parameters indicates that the probability for the magnitude greater than 0.7 is about 50%. Thus there is still large room for improvement for the prediction of tidal current in the presence of stratification and mesoscale background current.

In addition to the improvement of surface tidal current, the tidal current under the surface might also be better represented with improved stratification. Fig. 8 compares the tidal current ellipses at different depths with ADCP observations at mooring station 46092 (mooring M1) within Monterey Bay, whose position is shown as a red star in Fig. 6E. From Experiments 1–4, the magnitude of tidal current is gradually increased. The magnitudes of tidal current ellipses from Experiments 3 and 4 are comparable with those from observation. The minimum tidal current at the depth of 200–250 m is also reproduced in Experiment 4. Though there is a discrepancy in the phase of tidal current at the depth of 300–450 m, the overall improvement of tidal current simulation is obvious. Thus, for a given representation of bottom topography, the baroclinic tide simulation can be improved with a better representation of the stratification.

5.2. Tidal currents for different stratifications

The results of these four experiments indicate that the surface tidal current simulation is improved with better representation of stratification. In this subsection, the surface tidal current is separated into barotropic tidal current and baroclinic tidal current. The improvement of the surface tidal current is analyzed through changes in the barotropic tidal current and baroclinic tidal current at the surface. The spatial distribution of the M_2 barotropic tidal current ellipses shows some similarities among Experiments 2–4. (Fig. 9). For these three experiments, the tidal current ellipses are generally along isobaths, especially where the water depth is shallower than 200 m. The magnitude of the tidal current is reduced and the sense of rotation is counterclockwise within the submarine canyon where the water depth is greater than 1000 m. For Experiment 1, the surface tidal current and barotropic tidal current are roughly the same as expected since its density is constant. The magnitude of tidal current of Experiment 1 is much less than those with stratification. From Fig. 6E and Fig. 9, it may be concluded that the enhanced tidal currents on the shelf region are associated with barotropic tides and can be influenced by stratification.

As expected the baroclinic tidal current is negligible for Experiment 1, which has a constant density. With the presence of stratification the surface baroclinic tidal current tends to have a larger magnitude at the head of the canyon and in regions where the water depth is greater than 1000 m (Fig. 10B–D). In regions shallower than 200 m (except the canyon head), the baroclinic tidal currents tend to be weaker than those of the deeper region. The current ellipses tend to be at right angles to the isobaths, especially on the northern and southern flanks of the Monterey Submarine Canyon where the water depth is shallower than 200 m. In regions deeper than 1000 m, the surface baroclinic tidal current ellipses tend to be oriented in the direction of the canyon axis. The baroclinic tidal activity, as measured by the area-averaged depth-integrated baroclinic tidal energy, increases from 270 J m^{-2} for Experiment 2 to 358 J m^{-2} for Experiment 4. This is consistent with the increases in the magnitude of surface baroclinic tidal currents (Table 5). In Rosenfeld et al. (2008), their model runs with constant density and uniform stratification also indicate that the presence of stratification can greatly enhance the magnitude of the tidal current. From the above analysis, it may be concluded that the large surface tidal currents at the canyon head and the southwestern entrance of the canyon (Fig. 6E) are associated with baroclinic tide generation and propagation, as indicated in Figs. 5 and 10. The counterclockwise rotation of surface tidal current (Fig. 6E), on the other hand, might be related

Please cite this article as: Wang, X., et al., Modeling tides in Monterey Bay, California. Deep-Sea Research II (2008), doi:10.1016/j.dsr2.2008.08.012

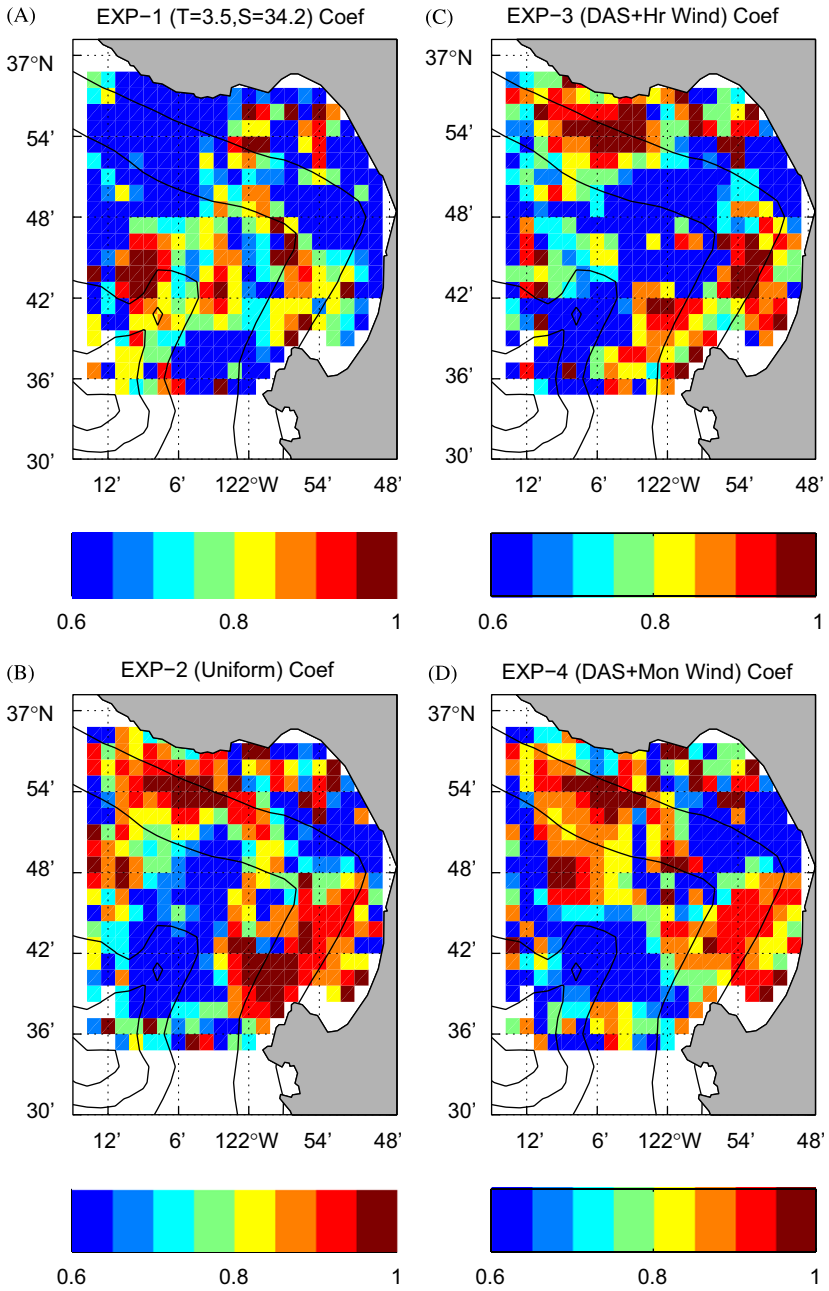

Fig. 7. The magnitude of complex correlation coefficient between model surface M_2 tidal current ellipses from four numerical experiments (A–D) and high-frequency radar observations of August 2003. The contours show selected (50, 200, 1000, 1500, 2000 m) model isobaths.

to both barotropic tides (Fig. 9) and baroclinic tides (Fig. 10). The result from the above four experiments indicates that both the barotropic and baroclinic tidal currents can be changed with the change in stratification. This seemingly surprising conclusion can be understood from the perspective that a clean separation between barotropic and baroclinic motions comes from the assumptions of flat bottom, linearity, and non-viscosity (Gill, 1982). Barotropic and baroclinic motions can be converted to each other when the above three assumptions are not satisfied, which is the case of Monterey Bay.

6. Conclusion

A three-dimensional, one-way nested ocean general circulation model is used to simulate tides along the central West Coast of the US. The goal of this work is to develop a tide-permitting coastal forecasting system. The outermost model domain covers the region from Southern California to Oregon, and the innermost domain zooms into Monterey Bay, California, with a horizontal resolution of 1.6 km and 32 vertical levels. The model can simulate barotropic tidal signals very well in these regions. The total discrepancy in the amplitudes of the eight major tide constituents, measured by the root of summed squares, is 3.6 cm in the Monterey Bay region and 5.4 cm along the US West Coast, which is about 10% of the amplitude of the most energetic M_2 constituent. For the major tidal constituents, the phase error is generally much less than 10°. Comparing tidal currents from models of similar resolution, however, the discrepancy for barotropic tidal current reaches over 30%. The general features of the surface tidal current in Monterey Bay, which reveal the baroclinic tidal activity in the region, can be reproduced by the model. However, there is much

Please cite this article as: Wang, X., et al., Modeling tides in Monterey Bay, California. Deep-Sea Research II (2008), doi:10.1016/j.dsr2.2008.08.012

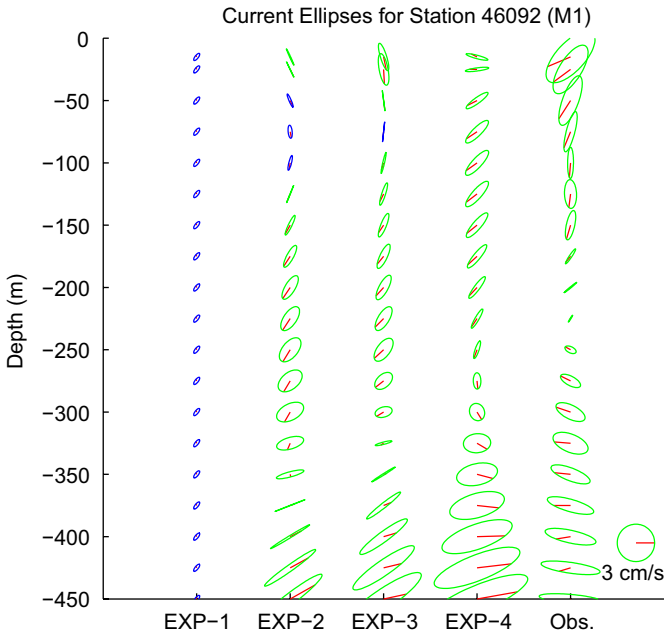

Fig. 8. Comparison of tidal current ellipses from Experiments 1–4 as defined in Fig. 6 and those from ADCP observations at mooring station 46092 (mooring M1 in Monterey Bay).

room for improvement in terms of magnitude and spatial pattern. For a given model configuration, our experiments demonstrate that realistic stratification can improve the surface tidal currents through changes in both the barotropic and baroclinic tidal currents. Subtle differences in stratification can cause significant changes in surface tidal currents.

The validation of surface tidal currents in the present research relies totally on the HF-radar observations, which provide spatial distributions of currents. The potential applications of HF-radar observations are demonstrated in their assimilation in circulation models (Paduan and Shulman, 2004) and tidal models (Kurapov et al., 2003). With more installations of HF radars along the coast, the data will become more important for coastal monitoring and forecasting. However, errors in the HF-radar observations can come from the spatial and temporal current variability and from the analysis of radar spectral data (Lipa, 2003). There is still a lack of knowledge regarding the uncertainties in such observations and how to make use of the information of these uncertainties. In terms of baroclinic tide generation and propagation, the resolutions of the innermost model domain are still too coarse in both the horizontal and vertical directions, and the model topography may be too smooth to simulate all the generation processes. These aspects will be improved in the next generation ROMS for the region, which is presently under development. The interaction of tides and background stratification and current fields, which is demonstrated in the numerical experiments, is beyond the scope

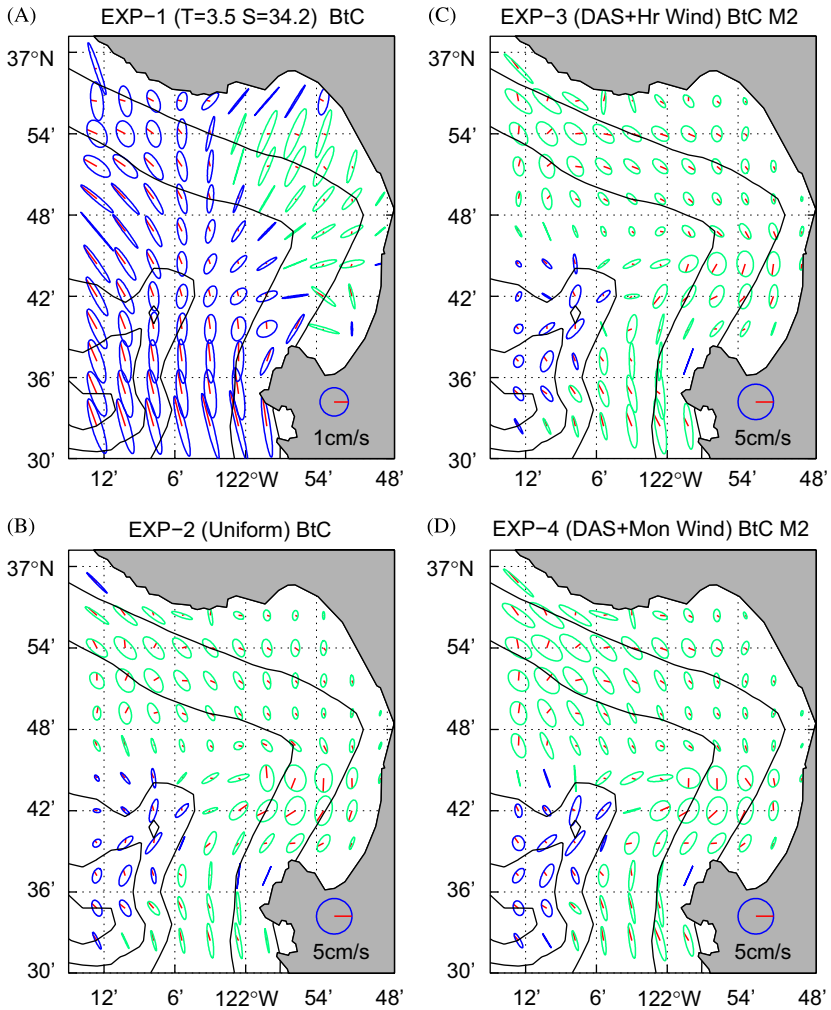

Fig. 9. Barotropic (depth-averaged) M_2 tidal current ellipses for the four experiments (A–D) defined in Fig. 6. The convention for plotting tidal current ellipses is the same as in Fig. 4. The contours show selected (50, 200, 1000, 1500, 2000 m) model isobaths.

Please cite this article as: Wang, X., et al., Modeling tides in Monterey Bay, California. Deep-Sea Research II (2008), doi:10.1016/j.dsr2.2008.08.012

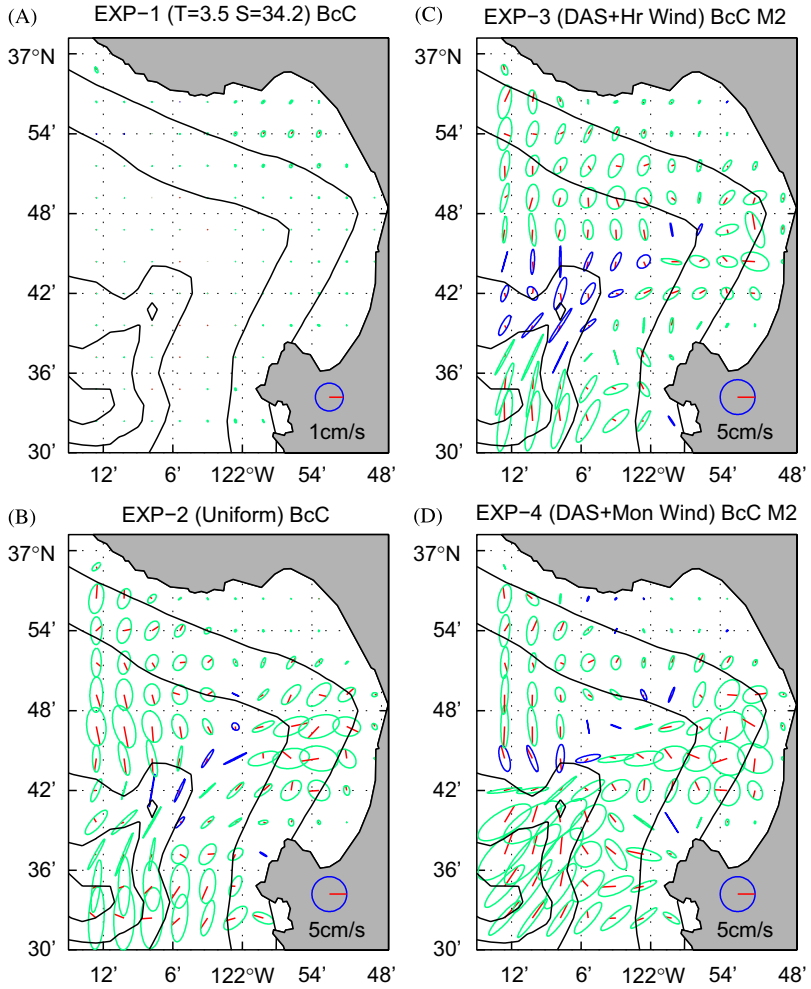

Fig. 10. Surface baroclinic (with depth-averaged current removed) M_2 tidal current ellipses for the four experiments (A–D) defined in Fig. 6. The convention for plotting tidal current ellipses is the same as in Fig. 4. The contours show selected (50, 200, 1000, 1500, 2000 m) model isobaths.

of present research and deserves a separate study. Nonetheless, the successful addition of tidal signals within the nested regional ocean general circulation model represents a significant step toward a tide-permitting forecasting system for the Monterey Bay region.

Acknowledgements

The research was carried out, in part, by the Jet Propulsion Laboratory (JPL), California Institute of Technology, under contract with the National Aeronautics and Space Administration. The financial support was provided by the Office of Naval Research through a subcontract from Monterey Bay Aquarium Research Institute to Raytheon, and NOAA COTS funding and California Coastal Conservancy through the COCMP program (both through subcontracts from Scripps Institution of Oceanography/UCSD to Raytheon). The long-term support from Drs. Emily Greene and Michael Lampel at the Pasadena office of Raytheon is acknowledged. Computations were performed on computers provided by the JPL Supercomputer Project and the NASA Advanced Supercomputing Division at Ames Research Center. High-frequency radar data were supported during this period by NOAA award No. NA160C2936 to the Center for Integrated Marine Technologies (CIMT). The authors would like to thank three anonymous reviewers for their insightful and detailed comments. XCW would like to thank Dr. Peggy Li, Mr. Quoc Vu, and Mrs. Hongchun Zhang for their technical help and Drs. C. K. Shum, Eric Kunze, Gary Egbert, and Mike Foreman for discussions.

Appendix A. Baroclinic tidal energy and energy flux

In a hydrostatic model, the energy equation for baroclinic waves can be written as (Gill, 1982)

$$\frac{\partial}{\partial t}\left[\frac{1}{2}\rho_0(u^2+v^2)+\frac{1}{2}\frac{g^2\rho'^2}{\rho_0 N^2}\right]+\frac{\partial}{\partial x}(p'u)+\frac{\partial}{\partial y}(p'v)=G+D, \quad (2)$$

in which ρ_0 is a reference density, N is buoyancy frequency, and p' and ρ' are the perturbation pressure and density, respectively. Here G and D are the generation and dissipation terms of baroclinic waves. The exact form and the calculation of these two terms are model dependent in order to achieve an accurate energy budget analysis (Kurapov et al., 2003). This subject is beyond the scope of present research.

To compute p', we start from the hydrostatic equation (Kunze et al., 2002; Cummins and Oey, 1997),

$$\frac{\partial p'}{\partial z}=-\rho' g. \quad (3)$$

Integrating the above equation from depth z to 0, we have

$$p'(z)=p'(0)+\int_z^0 \rho' g\,dz, \quad (4)$$

Please cite this article as: Wang, X., et al., Modeling tides in Monterey Bay, California. Deep-Sea Research II (2008), doi:10.1016/j.dsr2.2008.08.012

where we compute $p'(0)$ as

$$p'(0) = -\frac{1}{H}\int_{-H}^{0}\int_{z'}^{0} \rho' g \, dz \, dz'. \quad (5)$$

Eq. (5) leads to $\int_{-H}^{0} p'(z)\,dz = 0$. In our calculation, the horizontal velocity perturbations u and v are computed by removing the vertical averaged components. The kinetic energy in the vertical direction is ignored since this term is small in general. The amplitude and phase are estimated using the T_TIDE matlab package (Pawlowicz et al., 2002).

References

Althaus, A.M., Kunze, E., Sanford, R.B., 2003. Internal tide radiation from Mendocino Escarpment. Journal of Physical Oceanography 33, 1510–1527.

Baines, P.G., 1982. On internal tide generation models. Deep-Sea Research 29, 307–338.

Battisti, D.S., Clarke, A.J., 1982. A simple method for estimating barotropic tidal currents on continental margins with specific application to the M_2 tide off the Atlantic and Pacific Coasts of the United States. Journal of Physical Oceanography 12, 8–16.

Blayo, E., Debreu, L., 1999. Adaptive mesh refinement for finite-difference ocean models: first experiments. Journal of Physical Oceanography 29, 1239–1250.

Beckmann, A., Haidvogel, D.B., 1993. Numerical simulation of flow around a tall isolated seamount, Part 1: problem formulation and model accuracy. Journal of Physical Oceanography 23, 1736–1753.

Carter, G., Gregg, M.C., 2002. Intense, variable mixing near the head of Monterey Submarine Canyon. Journal of Physical Oceanography 32, 3145–3165.

Carter, G., Gregg, M.C., Lien, R.-C., 2005. Internal waves, solitary-like waves, and mixing on the Monterey Bay shelf. Continental Shelf Research 25, 1499–1520.

Chao, Y., Li, Z., Farrara, J., McWilliams, J.C., Bellingham, J., Capet, X., Chavez, F., Choi, J.-K., Davis, R., Doyle, J., Fratantoni, D.M., Li, P., Marchesiello, P., Moline, M.A., Paduan, J., Ramp, S., 2008. Development, implementation and evaluation of a data-assimilative ocean forecasting system off the central California coast. Deep-Sea Research II, this issue [doi:10.1016/j.dsr2.2008.08.011].

Chapman, D.C., 1985. Numerical treatment of cross-shelf open boundaries in a barotropic coastal model. Journal of Physical Oceanography 15, 1060–1075.

Cummins, P.F., Oey, L.-Y., 1997. Simulation of barotropic and baroclinic tides off northern British Columbia. Journal of Physical Oceanography 27, 762–781.

Egbert, G.D., Erofeeva, S.Y., 2002. Efficient inverse modeling of barotropic ocean tides. Journal of Atmospheric and Oceanic Technology 19, 183–204.

Egbert, G.D., Bennett, A.F., Foreman, M.G.G., 1994. TOPEX/POSEIDON tides estimated using a global inverse model. Journal of Geophysical Research 99, 24821–24852.

Emery, W.J., Thomson, R.E., 2004. Data analysis methods in physical oceanography. Elsevier, 638pp.

Flather, R.A., 1976. A tidal model of the north-west European continental shelf. Memoires de la Societe Royale des Sciences de Liege 6, 141–164.

Foreman, M.G.G., 1977. Manual for tidal height analysis and prediction. Pacific Marine Science Report 77-10, Institute of Ocean Sciences, Patricia Bay, Sidney, BC, 97pp.

Foreman, M.G.G., 1978. Manual for tidal currents analysis and prediction. Pacific Marine Science Report 78-6, Institute of Ocean Sciences, Patricia Bay, Sidney, BC, 57pp.

Foreman, M.G.G., Henry, R.F., Walters, R.A., Ballantyne, V.A., 1993. A finite element model for tides and resonance along the north coast of British Columbia. Journal of Geophysical Research 98, 2509–2531.

Gill, A.E., 1982. Atmosphere-Ocean a Dynamics. Academic Press, New York, 662pp.

Gordon, R.L., Marshall, N.F., 1976. Submarine canyons: internal wave traps? Geophysical Research Letters 3, 622–624.

Gregg, M.C., Carter, G.S., Kunze, E., 2005. Corrigendum. Journal of Physical Oceanography 35, 1712–1715.

He, R., Wilkin, J.L., 2006. Barotropic tides on the southeast New England Shelf: a view from a hybrid data assimilative modeling approach. Journal of Geophysical Research C08002, doi:10.1029/2005JC003254.

Hodur, R.M., 1997. The Naval Research Laboratory's coupled ocean/atmosphere mesoscale prediction system (COAMPS). Monthly Weather Review 125, 1414–1430.

Holloway, P.E., Merrifield, M.A., 1999. Internal tide generation by seamounts, ridges, and islands. Journal of Geophysical Research 104, 25937–25951.

Jachec, S.M., Fringer, O.B., Gerritsen, M.G., Street, R.L., 2006. Numerical simulation of internal tides and the resulting energetics within Monterey Bay and the surrounding area. Geophysical Research Letters 33, L12605.

Kondo, J., 1975. Air-sea bulk transfer coefficients in diabetic conditions. Boundary-Layer Meteorology 9, 91–112.

Kundu, P.K., 1976. Ekman veering observed near the ocean bottom. Journal of Physical Oceanography 6, 238–242.

Kunze, E., Rosenfeld, L.K., Carter, G.S., Gregg, M.C., 2002. Internal waves in Monterey Submarine Canyon. Journal of Physical Oceanography 32, 1890–1913.

Kurapov, A.L., Egbert, G.D., Allen, J.S., Miller, R.N., Erofeeva, S.Y., Kosro, P.M., 2003. The M_2 internal tide off Oregon: inferences from data assimilation. Journal of Physical Oceanography 33, 1733–1757.

Large, W.G., Pond, S., 1982. Sensible and latent heat flux measurements over the ocean. Journal of Physical Oceanography 12, 464–482.

Large, W.G., McWilliams, J.C., Doney, S.C., 1994. Oceanic vertical mixing: a review and a model with nonlocal boundary layer parameterization. Reviews of Geophysics 32, 363–403.

Li, Z., Chao, Y., McWilliams, J.C., Ide, K., 2008a. A three-dimensional variational data assimilation scheme for the regional ocean modeling system. Journal of Atmospheric and Oceanic Technology, in press.

Li, Z., Chao, Y., McWilliams, J.C., Ide, K., 2008b. A three-dimensional variational data assimilation scheme for the regional ocean modeling system: implementation and experiments. Journal of Geophysical Research 113, C05002, doi:10.1029/2006JC004042.

Lien, R.-C., Gregg, M.C., 2001. Observations of turbulence in a tidal beam and across a coastal ridge. Journal of Geophysical Research 106, 4575–4591.

Lipa, B., 2003. Uncertainties in seasonde current velocities. In: Proceedings of the IEEE/OES Seventh Working Conference on Current Measurement Technology, pp. 95–100.

Luettich, R.A., Westerink, J.J., Scheffner, N.W., 1992. ADCIRC: an advanced three-dimensional circulation model for shelves, coasts and estuaries. Report I: theory and methodology of ADCIRC-2DDI and ADCIRC-3DL. Dredging Research Program Technical Report DRP-92-6, US Army Engineer Research and Development Center, Vicksburg, MS.

Marchesiello, P., McWilliams, J.C., Shchepetkin, A., 2001. Open boundary condition for long-term integration of regional oceanic models. Ocean Modelling 3, 1–21.

Nash, J., Alford, M.H., Kunze, E., 2005. Estimating internal wave energy fluxes in the ocean. Journal of Atmospheric and Oceanic Technology 22, 1551–1570.

Orlanski, I., 1976. A simple boundary condition for unbounded hyberbolic flows. Journal of Computational Physics 21, 251–269.

Paduan, J.D., Cook, M.S., 1997. Mapping surface currents in Monterey Bay with CODAR-type HF radar. Oceanography 10, 49–52.

Paduan, J.D., Shulman, I., 2004. HF radar data assimilation in the Monterey Bay area. Journal of Geophysical Research 109, C07S09.

Pawlowicz, R., Beardsley, R., Lentz, S., 2002. Classical tidal harmonic analysis including error estimates in MATLAB using T_TIDE. Computers & Geosciences 28, 929–937.

Penven, P., Debreu, L., Marchesiello, P., McWilliams, J.C., 2006. Evaluation and application of the ROMS 1-way embedding procedure to the central California upwelling system. Ocean Modelling 12, 157–187.

Petruncio, E.T., 1996. Observations and modeling of the internal tide in a submarine canyon. Ph.D. Dissertation, Department of Oceanography, Naval Postgraduate School, 181pp.

Petruncio, E.T., Rosenfeld, L.K., Paduan, J.D., 1998. Observations of the internal tide in Monterey Canyon. Journal of Physical Oceanography 28, 1873–1903.

Petruncio, E.T., Paduan, J.D., Rosenfeld, L.K., 2002. Numerical simulations of the internal tide in a submarine canyon. Ocean Modelling 4, 221–249.

Rainville, L., Pinkel, R., 2006. Propagation of low-mode internal waves through the ocean. Journal of Physical Oceanography 36, 1220–1235.

Ray, R., Mitchum, G., 1996. Surface manifestation of internal tides generated near Hawaii. Geophysical Research Letters 28, 1259–1262.

Raymond, W.H., Kuo, H.L., 1984. A radiation boundary condition for multi-dimensional flows. Quarterly Journal of the Royal Meteorological Society 110, 535–551.

Rosenfeld, L., Paduan, J., Petruncio, E.T., Goncalves, J.E., 1999. Numerical simulations and observations of the internal tide in a submarine canyon. In: Proceedings of 'Aha Huliko' a Hawaiian Winter Workshop, University of Hawaii at Manoa, 19–22 January, pp. 63–71.

Rosenfeld, L., Shulman, I., Cook, M., Paduan, J., Shulman, L., 2008. Methodology for a regional tidal model evaluation, with application to central California. Deep-Sea Research II, this issue [doi:10.1016/j.dsr2.2008.08.007].

Shchepetkin, A., McWilliams, J.C., 2005. The regional oceanic modeling system (ROMS): a split-explicit, free-surface, topography-following-coordinate ocean model. Ocean Modelling 9, 347–404.

Shum, C.K., Woodworth, P.L., Andersen, O.B., Egbert, G., Francis, O., King, C., Klosko, S., Le Provost, C., Li, X., Molines, J.M., Parke, M., Ray, R., Schlax, M., Stammer, D., Thierney, C., Vincent, P., Wunsch, C., 1997. Accuracy of recent ocean tide models. Journal of Geophysical Research 102, 15194–25173.

Smith, W.H.F., Sandwell, D.T., 1997. Global seafloor topography from satellite altimetry and ship depth soundings. Science 277, 1957–1962.

Song, Y.T., Haidvogel, D., 1994. A semi-implicit ocean circulation model using a generalized topography-following coordinate system. Journal of Computational Physics 115, 228–244.

Spargo, E.A., Westerink, J.J., Luettich, R.A., Mark, D.J., 2004. ENPAC 2003: a tidal constituent database for Eastern North Pacific Ocean. US Army Corps of Engineers, ERDC/CHL TR-04-12.

Please cite this article as: Wang, X., et al., Modeling tides in Monterey Bay, California. Deep-Sea Research II (2008), doi:10.1016/j.dsr2.2008.08.012